Journal of Materials Chemistry C

Accepted Manuscript

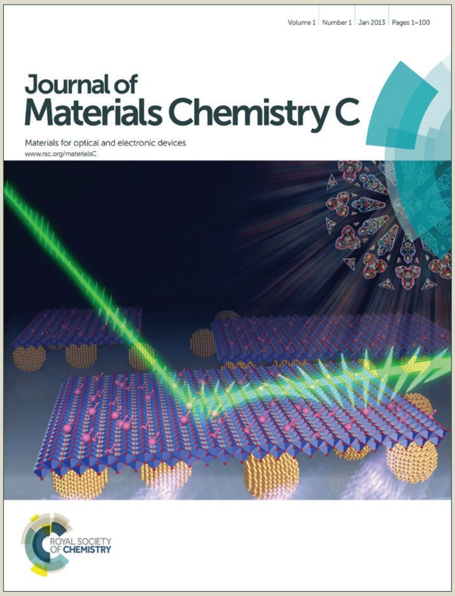

ROYAL SOCIETY OF CHEMISTRY

www.rsc.org/materialsC

Journal Name

ARTICLE

Fluorescence behavior of 5,10-disubstituted [5]helicene derivatives in solution and the effect of self-assembly on their radiative and non-radiative rate constants†

Received 00th January 20xx,
Accepted 00th January 20xx

DOI: 10.1039/x0xx00000x

www.rsc.org/

Takashi Hirose,[a] Natsuki Ito,[a] Hiromu Kubo,[a] Tohru Sato[b,c] and Kenji Matsuda*[a]

The surrounding environment of molecular fluorophore is one of the most important determining factor in luminescent properties, such as emission quantum yield, lifetime of the excited state, and color of luminescence. In this work, we investigate the relationship between self-assembled structure and the fluorescence properties of [5]helicene derivatives in solution phase. [5]Helicene derivative bearing tri(ethylene glycol) group formed spherical aggregates in aqueous media and that bearing (3,4,5-trioctyloxyphenyl)carbamoyl group formed fibrous aggregates in apolar solvent. Analysis based on the radiative (k_f) and non-radiative (k_{nr}) rate constants suggests that (1) an aggregation-induced suppression of fluorescence observed in aqueous media is attributed to the decrease of k_f and (2) an aggregation-induced enhancement of fluorescence observed for fibrous aggregates formed in an apolar solvent is associated with the suppression of k_{nr}, (3) [5]helicenes becomes almost non-fluorescent especialy in a polar solvent by introducing appropriate donor substituent due to a charge-transfer (CT) type property in the lowest energy excited state, and (4) the strong quenching effect due to the CT-type excitation can be efficiently alleviated by several approaches, such as by forming aggregates with an appropriate self-assembly motif or by controlling the energy level of molecular orbital.

1 Introduction

Helicenes are *ortho*-fused polycyclic aromatic compounds with a nonplanar screw-shaped skeleton, which have attracted attention in terms of the (enantioselective) organic synthesis[1–9] and their unique chiroptical properties, such as circular dichroism (CD) and circular polarized luminescence (CPL).[10–13] The CPL property closely associated with their helically twisted π-electrons is very attractive, however, fluorescence quantum yield of non-substituted [*n*]helicenes is typically very low ($\Phi_f < 0.05$ for [*n*]helicenes longer than $n = 5$),[14] which is due to a rapid intersystem crossing generating non-luminescent triplet state.[15,16] To overcome this drawback, considerable efforts has been devoted to design a highly luminescent helicene derivative.[17–25] Among pure [*n*]carbohelicene derivatives, to the best of our knowledge, the highest Φ_f value of 0.27 was reported for a push-pull-type substituted helicene derivative, i.e., 3,12-dimethoxy-7,8-dicyano-[5]helicene, in solution.[22]

Self-assembly of molecules has a great effect on their electronic states and the manner of relaxation pathways in the ground and excited states, therefore unprecedented chiroptical properties can be realized based on supramolecular chemistry.[1,4,26–32] Katz et al. reported that a [6]helicene-bisquinone derivative consisting of *p*-benzoquinone structure at either terminal of the helical core forms fibrous aggregates and exhibits a strong enhancement of nonlinear optical (NLO) properties in its multi-layered Langmuir-Blodgett (LB) film state.[27,28] Kawai et al. recently reported that the degree of anisotropy in CPL can be substantially enhanced by a controlled self-assembly of chiral organic chromophores.[32]

In this study, we synthesized [5]helicene derivatives bearing tri(ethylene glycol) group (**2a**) or tri(octyloxy)phenyl group (**3a**, **3b**) at the 5- and 10-positions and investigated their fluorescence properties changing upon self-assembly in solution (Fig. 1).

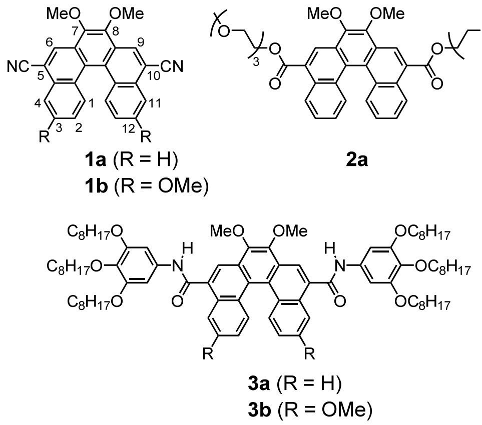

1a (R = H)
1b (R = OMe)

2a

3a (R = H)
3b (R = OMe)

Fig. 1 Chemical structures of 5,10-disubstituted [5]helicene derivatives.

---

[a] Department of Synthetic Chemistry and Biological Chemistry, Graduate School of Engineering, Kyoto University, Katsura, Nishikyo-ku, Kyoto 615-8510, Japan. E-mail: kmatsuda@sbchem.kyoto-u.ac.jp

[b] Department of Molecular Engineering, Graduate School of Engineering, Kyoto University, Katsura, Nishikyo-ku, Kyoto 615-8510, Japan.

[c] Unit of Elements Strategy Initiative for Catalysts & Batteries, Kyoto University, Katsura, Nishikyo-ku, Kyoto 615-8510, Japan.

† Electronic Supplementary Information (ESI) available: [details of any supplementary information available should be included here]. See DOI: 10.1039/x0xx00000x

Importantly, we have previously reported that electron withdrawing group (such as cyano and carbonyl substituents) introduced at the 5- and 10-positions removes molecular orbital degeneracy of [5]helicene and effectively suppresses the formation of benzo[*ghi*]perylenes by prohibiting cyclodehydrogenation reaction upon UV light irradiation.[9] Consequently, the luminescent property of [5]helicene derivatives can be carefully investigated using the photostable 5,10-disubstituted [5]helicenes.

2 Experimental

2.1 Synthesis of Materials

Unless specifically mentioned, reagents and solvents were obtained from commercial suppliers and used without further purification. All reactions were monitored by thin-layer chromatography carried out on 0.2 mm Merck silica gel plates (60F-254). Column chromatography was performed on silica gel (Nakalai Tesque, 70–230 mesh) or on a Biotage Instrument (Isolera One) with a SNAP flash silica gel cartridge (KP-Sil). Photoirradiation was performed using USHIO 500 W super-high-pressure mercury lamp. Final products were purified by HPLC (Kanto chemical, Mightysil RP-18GP 250–20, 5 μm). ^{1}H and ^{13}C NMR spectra were recorded on a JEOL JNM-ALPHA500 instrument at room temperature. Proton chemical shifts were reported in ppm downfield from tetramethylsilane (TMS) as an internal standard. Mass spectra were obtained by a Thermo Scientific Exactive mass spectrometer (ESI-Orbitrap) and a Thermo Scientific LTQ orbitrapXL mass spectrometer (MALDI-Orbitrap). Dithranol was used as the matrix of MALDI. Melting points were measured with a Yanaco MP-500P apparatus and were not corrected. Ethanol was refluxed in the presence of magnesium and iodine, and then distilled. Toluene and dimethylformamide (DMF) was dried over calcium hydride and distilled before use. 2,3-Dimethoxyterephthalaldehyde were prepared according to the literature.[33] 5,10-Dicyano-7,8-dimethoxy[5]helicene (**1a**) and 7,8-dimethoxy[5]helicene-5,10-dicarboxylic acid (**4a**) have reported in a literature.[9]

5,10-bis(2-(2-(2-methoxyethoxy)ethoxy)ethoxycarbonyl)-7,8-dimethoxy[5]helicene (2a). To a stirred solution of 7,8-dimethoxy[5]helicene-5,10-dicarboxylic acid (**4a**)[9] (100 mg, 0.23 mmol) in dry DMF (2 mL) was added *N*,*N*-dimethyl-4-aminopyridine (DMAP) (15 mg, 0.12 mmol) and triethyleneglycol monomethylether (0.2 mL). *N*,*N*'-dicyclohexylcarbodiimide (DCC) (200mg, 0.95mmol) was added to the solution at 0 °C, then the reaction mixture was stirred for 5 min at 0 °C and 12 h at room temperature. Precipitated urea was removed by filtration. The filtrate was poured into water and extracted with ethyl acetate. The combined organic layers were washed with aq. HCl (1 N) and aq. $NaHCO_3$, dried over $MgSO_4$ and filtered. The crude product was concentrated in vacuo and was purified by silica gel column chromatography (eluent: ethyl acetate). Further purification by HPLC gave compound **2a** as a yellow oil (25 mg, 0.035 mmol, 15%). ^{1}H NMR ($CDCl_3$, 500 MHz, δ) 3.35 (6H, s), 3.56–3.52 (4H, m), 3.69–3.66 (4H, m), 3.76–3.72 (4H, m), 3.83–3.80 (4H, m), 3.99 (4H, *t*, *J* = 5 Hz), 4.16 (6H, s), 4.75–4.63 (4H, m), 7.56 (2H, *t*, *J* = 8 Hz), 8.31 (2H, *d*, *J* = 8 Hz), 8.61 (2H, *t*, *J* = 9 Hz), 8.81 (2H, *d*, *J* = 9 Hz), 8.96 (2H, s); ^{13}C NMR ($CDCl_3$, 126 MHz, δ) 59.0, 61.3, 64.5, 69.3, 70.6, 70.7, 70.8, 71.9, 124.6, 125.1, 125.8, 126.5, 127.2, 127.7, 128.0, 129.0, 129.2, 131.4, 145.3, 167.5; ESI-HRMS *m*/*z* $[M + Na]^+$ calcd for $C_{40}H_{46}O_{12}Na^+$, 741.2881; found, 741.2851; ε_{max} = 3.1 × 10^4 M^{-1}cm^{-1} (in acetonitrile at 319 nm); $\lambda_{max,abs}$ = 323 nm in water/MeCN = 99/1 (v/v).

5,10-bis(3,4,5-trimethoxyphenylcarbamoyl)-7,8-dimethoxy[5]helicene (3a). To a solution of 7,8-dimethoxy[5]helicene-5,10-dicarboxylic acid (**4a**)[9] (86 mg, 0.20 mmol) and 3,4,5-trioctyloxyaniline[34] (310 mg, 0.65 mmol) in dry DMF (2 mL) were added *N*,*N*'-dicyclohexylcarbodiimide (DCC) (165 mg, 0.80 mmol) and 1-hydroxybenzotriazole (HOBt) (55 mg, 0.41 mmol). The reaction mixture was stirred at room temperature for 22 h. The mixture was poured into aq. HCl (1 N) and extracted with ethyl acetate. The combined organic layers were washed with aq. HCl (1 N), aq. $NaHCO_3$, and water, dried over $MgSO_4$, filtered and concentrated in vacuo. The crude product was purified by silica gel column chromatography (hexane/CH_2Cl_2 = 50/50–0/100) to afford a fraction containing the desired product. Further purification by a recycle GPC gave compound **3a** as a yellow solid (160 mg, 0.12 mmol, 60%). ^{1}H NMR ($CDCl_3$, 500 MHz, δ) 0.87–0.92 (18H, m), 1.30–1.50 (60H, m), 1.74–1.87 (12H, m), 3.94–4.10 (12H, m), 4.16 (6H, s), 7.07 (4H, s), 7.31 (2H, *t*, *J* = 7.9 Hz), 7.57 (2H, *t*, *J* = 7.6 Hz), 7.84 (2H, s), 8.39 (2H, *t*, *J* = 8.3 Hz), 8.42 (2H, *t*, *J* = 8.6 Hz), 8.55 (2H, s); ^{13}C NMR ($CDCl_3$, 126 MHz, δ) 14.01, 14.03, 22.60, 22.63, 26.05, 26.08, 29.2, 29.3, 29.5, 30.2, 31.77, 31.84, 61.1, 69.1, 73.5, 98.9, 119.1, 125.3, 127.0, 127.6, 128.4, 129.1, 131.1, 133.7, 134.5, 135.1, 145.1, 153.2, 167.1; MALDI-HRMS *m*/*z* $[M + Na]^+$ calcd for $C_{86}H_{124}N_2O_{10}Na^+$: 1367.9148; found: 1367.9118; mp 177–179 °C; ε_{max} = 4.5 × 10^4 M^{-1}cm^{-1} (in chloroform at 321 nm); $\lambda_{max,abs}$ = 319 nm in MCH, 318 nm in haptane.

5,10-bis(3,4,5-trimethoxyphenylcarbamoyl)-3,7,8,12-tetramethoxy[5]helicene (3b). To a suspension of 5,10-dicyano-3,7,8,12-tetramethoxy[5]helicene (**1b**) (90 mg, 0.20 mmol) in ethanol (6 mL) was added aq. NaOH (10 M, 6 mL). The mixture was refluxed for 30 h. After cooling to room temperature, the resulting solution was acidified by conc. HCl. The precipitate was filtrated and washed with water to afford a pale yellow powder of dicarboxylic acid derivative (**4b**) (180 mg). The yellow powder was used for the next step without further purification. The observed yellow powder (180 mg) and 3,4,5-trioctyloxyaniline[34] (290 mg, 0.60 mmol) were dissolved into dry DMF (2 mL) and then 1-ethyl-3-(3-dimethylaminopropyl)-carbodiimide hydrochloride (EDC) (150 mg, 0.80 mmol) and HOBt (57 mg, 0.42 mmol) were added to the solution. The reaction mixture was stirred at room temperature for 4 days. The mixture was poured into aq. HCl (1 N) and extracted with ethyl acetate. The combined organic layers were washed with aq. HCl (1 N), aq. $NaHCO_3$, and brine, dried over $MgSO_4$, filtered and concentrated in vacuo. The crude product was purified by silica gel column chromatography (Biotage, Zip 10 g, hexane/dichloromethane/methanol =

50/50/0–0/100/0–0/90/10) to afford a fraction containing the desired product as a brown amorphous. Further purification by a recycle GPC gave compound **3b** as a brown solid (37 mg, 0.026 mmol, 13%). ^{1}H NMR ($CDCl_3$, 500 MHz, δ) 0.87–0.92 (18H, m), 1.30–1.45 (48H, m), 1.50–1.65 (12H, m), 1.74–1.88 (12H, m), 3.96–4.08 (12H, m), 4.13 (6H, s), 6.93 (2H, *dd*, J = 9.3 and 2.6 Hz), 7.05 (4H, s), 7.80 (2H, *d*, J = 2.5 Hz), 7.92 (2H, s), 8.22 (2H, *d*, J = 9.2 Hz), 8.51 (2H, s); ^{13}C NMR ($CDCl_3$, 126 MHz, δ) 14.1, 22.66, 22.69, 26.10, 26.14, 29.3, 29.4, 29.6, 30.3, 31.8, 31.9, 55.5, 61.2, 69.2, 73.6, 99.1, 104.5, 116.7, 119.9, 125.5, 126.1, 126.4, 130.1, 130.5, 133.6, 133.7, 135.3, 144.4, 153.4, 158.4, 167.3; MALDI-HRMS m/z $[M + Na]^+$ calcd for $C_{88}H_{128}N_2O_{12}Na^+$: 1427.9359; found: 1427.9376; mp 181–183 °C; $\varepsilon_{max} = 4.7 \times 10^4$ $M^{-1}cm^{-1}$ (in chloroform at 333 nm); $\lambda_{max,abs}$ = 331 nm in MCH, 330 nm in haptane.

2.2 Preparation of aggregates in solution phase

For aqueous solution of compound **2a**, an acetonitrile solution of **2a** (3 mL) at a target concentration ($c = 1 \times 10^{-5}$ M) was prepared and its precise concentration was confirmed by UV-vis absorption spectroscopy. After removal of solvent under reduced pressure, the compound was dissolved in a small amount of acetonitrile (0.03 mL). A large amount of water (2.97 mL) was then added to the solution, providing aqueous solution of **2a** at a specific concentration (water/acetonitrile = 99/1, v/v). For heptane solution of compound **3a** and **3b**, a chloroform solution of the compound (4 mL) at a target concentration ($c = 1 \times 10^{-4}$ M) was prepared and its precise concentration was confirmed by UV-vis absorption spectroscopy. After removal of solvent under reduced pressure, the same amount of heptane (4 mL) was added to the remaining compound in a flask. Because of the low solubility of compound **3a** in heptane, the prepared heptane solution was sonicated for 10 minutes at 40 °C before spectroscopic measurements.

3 Results and discussion

Molecular design and synthesis

Two different approaches forming self-assembled structures were investigated to assess the effect of self-assembly on the fluorescence behavior of [5]helicenes: one is spherical aggregates formed by hydrophobic interactions in aqueous environment and the other is fibrous aggregates formed by van der Waals interactions in apolar solvent. As a helical core structure, we chose 5,10-disubstituted [5]helicenes because of their ease of synthesis and high photostability. We have recently reported that 5,10-dicyano-7,8-dimethoxy[5]helicene (**1a**) can be obtained via a facile one-pot reaction of 2,3-dimethoxyterephthalaldehyde with benzyl cyanide using Knoevenagel reaction followed by photocyclodehydrogenation in 72% overall yield.[9] Methoxy group at the 7- and 8-positions imparts a good solubility to [5]helicene core in common organic solvents.

A key precursor, 5,10-dicarboxy substituted derivative (**4a**), was synthesized in 93% yield by hydrolysis of compound **1a** in the presence of sodium hydroxide. Starting from the key precursor of dicarboxylic acid, various substituents can be introduced at the 5- and 10-positions via conventional esterification or amidation reactions. In this work, compound **2a** bearing methoxy-terminated tri(ethylene glycol) chain and **3a** bearing (3,4,5-trioctyloxyphenyl)carbamoyl group were synthesized as shown in scheme 1. Methoxy-terminated oligo(ethylene glycol) and 3,4,5-trialkoxyphenyl groups are commonly used substituents to design self-assembly of organic molecules based on non-covalent interactions in solution phase.[35–39] 3,7,8,12-Tetramethoxy-[5]helicene derivative **3b** was also synthesized in the same method to assess the effect of methoxy group introduced at the 3- and 12-positions on self-assembly and its fluorescence behavior. Indeed, we found that the two additional methoxy group improves fluorescence property of [5]helicenes in the monomer state (see below).

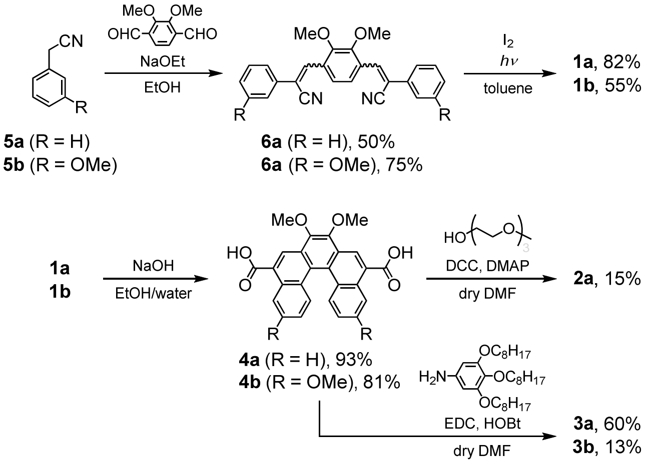

Scheme 1 Synthesis of 5,10-disubstituted [5]helicene derivatives.

UV-vis. absorption

UV-vis absorption spectrum of **2a** bearing tri(ethylene glycol) chain was measured in acetonitrile (MeCN) and an aqueous media at the same concentration ($c = 1 \times 10^{-5}$ M) (Fig. 2a).

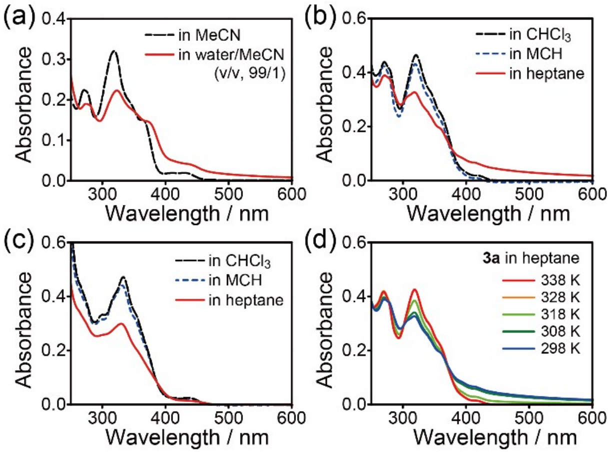

Fig. 2 Absorption spectra of (a) compound **2a** ($c = 1 \times 10^{-5}$ M; red solid line, water/MeCN = 99/1; black dashed line, MeCN), (b) **3a** ($c = 1 \times 10^{-4}$ M; red solid line, *n*-heptane; blue dotted line, MCH; black dashed line, $CHCl_3$), and (c) **3b** ($c = 1 \times 10^{-4}$ M; red solid line, *n*-heptane; blue dotted line, MCH; black dashed line, $CHCl_3$) measured at 298 K. (d) Temperature dependent absorption spectra of **3a** in heptane ($c = 1 \times 10^{-4}$ M).

Compound **2a** has a strong absorption band whose wavelength maximum is observed at 319 nm in MeCN. A weak band appeared around 420 nm and absorption edge was observed at ca. 450 nm. Because compound **2a** is not soluble in pure water, aqueous solution of **2a** was prepared by adding excess amount of water to a concentrated MeCN solution of **2a** (water/MeCN = 99/1, v/v). In an aqueous solution thus prepared, magnitude of absorbance around 320 nm significantly decreased and absorption edge extended to more than 600 nm where compound **2a** has no adsorption. The extension of absorption edge is probably due to the effect of scattering from aggregates whose size is comparable to or larger than the wavelength of visible light. These unique behaviors in aqueous solution suggest the formation of aggregates of **2a**.

Absorption spectra of **3a** and **3b** bearing (3,4,5-trioctyloxyphenyl)carbamoyl group were measured in chloroform ($CHCl_3$), methylcyclohexane (MCH), and heptane at the same concentration (c = 1 × 10^{-4} M) (Fig. 2b and c). Prominent scattering effect appeared only for compound **3a** in heptane on the absorption spectrum around 400 to 600 nm. Although the scattering effect was not clear for compound **3b**, the absorbance at 250 to 400 nm was significantly small in heptane out of the three solvent. These results indicate the formation of aggregates of **3a** and **3b** in heptane. Interestingly, for both compounds **3a** and **3b**, absorption spectrum in MCH is similar to that in $CHCl_3$ rather than that in heptane, suggesting that aggregation behavior of compounds **3a** and **3b** is very sensitive to the molecular structure of solvent; they are molecularly dispersed in cyclic apolar solvent (i.e., MCH), but form aggregates in linear apolar solvent (i.e., heptane). Such supramolecular system that is strongly sensitive to a subtle difference in solvent geometry has been previously reported by several groups.[40,41]

When the solution of **3a** in heptane was heated from 298 to 338 K, the scattering effect around 400 to 600 nm diminished and the magnitude of absorption band around 300 to 350 nm increased. Thus, the spectrum in heptane at higher temperature (T = 338 K) is similar in shape to the spectrum in MCH at 298 K. The result of spectral change upon heating supports the fact that compound **3a** does not form any aggregates in MCH but form aggregates in heptane. Similar temperature dependence was also observed for compound **3b** in heptane (Fig. S1 in the ESI†).

Macroscopic morphologies

The manner of molecular arrangement and intermolecular interactions inside the aggregates should be strongly associated with the photophysical property in the aggregated state. To assess the macroscopic morphology and size of aggregates composed of compounds **2a**, **3a**, and **3b**, transmission electron microscopy (TEM) measurements were carried out. The samples for TEM measurements were prepared from solution in which aggregates are formed (i.e., **2a**, from water/MeCN = 99/1; **3a** and **3b**, from heptane solution).

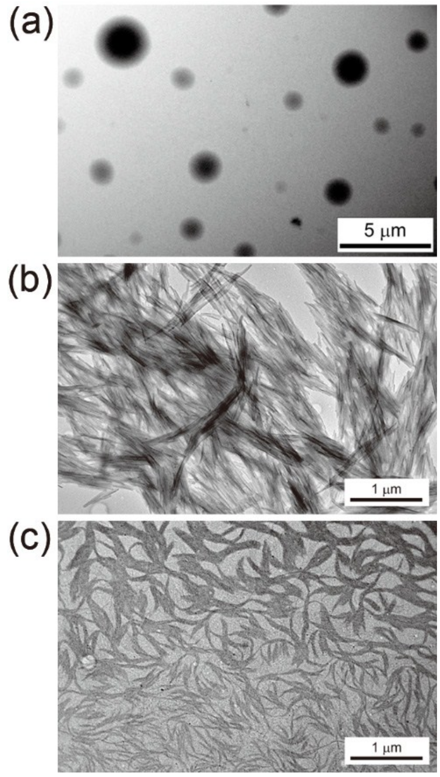

Fig. 3 TEM images of aggregates of (a) compound **2a** (×2.5 k), compound **3a** (×10 k), and (c) compound **3b** (×10 k) prepared from solution in which aggregates form (**2a**, from water/MeCN = 99/1; **3a** and **3b**, from heptane solution). The sample of **2a** was stained with OsO_4 vapor.

As shown in Fig. 3a, a spherical structure composed of compound **2a** is formed in aqueous media. The averaged diameter (d) of spheres was determined as $d = 1.0 \pm 0.6$ μm based on a histogram of totally 317 spheres that was fitted by a log-normal distribution (Fig. S6 in the ESI†). The size determined by TEM observation was significantly larger than that suggested by dynamic light scattering (DLS) measurement; the number-weighted average size was 80 ± 20 nm based on DLS measurement of the aqueous solution of **2a** (Fig. S7 in the ESI†). Thus, TEM measurement suggests that compound **2a** forms spherical aggregates by hydrophobic interactions in aqueous media and the size of aggregates has a large distribution ranging from several tens of nanometers to several micrometers.

In contrast to the spherical morphology of compound **2a**, compounds **3a** and **3b** form characteristic fibrous aggregates in heptane by van der Waals interactions (Fig. 3b and c). Despite the similarity in its chemical structure between **3a** and **3b**, a clear difference was found in the macroscopic morphologies of their aggregates. Compound **3a** having two methoxy group at 7- and 8-positions forms a rigid fibrous structure whose width is around 50 nm and length is around 500 nm to 1 μm (aspect ratio is roughly 1:10) (Fig. 3b and S8 in the ESI†). On the other hand, an entangled leaf-like morphology was observed for compound **3b** bearing the additional two methoxy groups at the 3- and 12-

positions (Fig. 3c and S9 in the ESI†), suggesting that aggregates composed of **3b** is less rigid than those of **3a**. The size of the leaf-like pattern was different depending on the region of interest; for example, the size is around 100 nm in width and 500 nm in length at the upper part of Fig. 3c (aspect ratio is roughly 1:5), while 20 nm in width and 200 nm in length at the bottom part of Fig. 3c (aspect ratio is roughly 1:10).

Fluorescence change upon aggregation

The change of fluorescence property of compounds **2a**, **3a**, and **3b** upon aggregation was carefully investigated in solution phase. Photographs of emitting solutions under UV light irradiation (λ_{irrad} = 365 nm) and corresponding fluorescence spectra are shown in Fig. 4 and 5, respectively. Compound **2a** shows a green emission in MeCN ($\lambda_{max,FL}$ = 493 nm) and fluorescence quantum yield (Φ_f) is 17% in the monomer state in dilute solution (Fig. 4a and 5a). When spherical aggregates are formed in aqueous media, fluorescence quantum yield slightly decreased to 13% and maximum wavelength of fluorescence band was red-shifted by 14 nm ($\lambda_{max,FL}$ = 507 nm). Thus, aggregation-induced suppression of fluorescence was observed for compound **2a**.

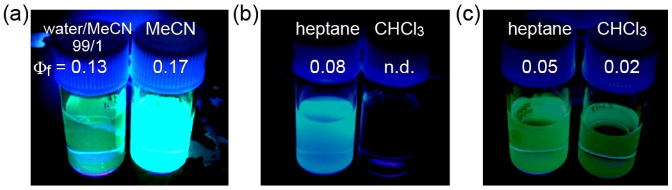

Fig. 4 Pictures of emitting solution of (a) compounds **2a** (left, water/MeCN = 99/1; right, MeCN), (b) **3a** (left, heptane; right, $CHCl_3$), and (c) **3b** (left, heptane; right, $CHCl_3$) under UV light irradiation (λ_{irrad} = 365 nm). The emission color coordinates on CIE 1931 diagram is shown in Fig. S10 in the ESI†.

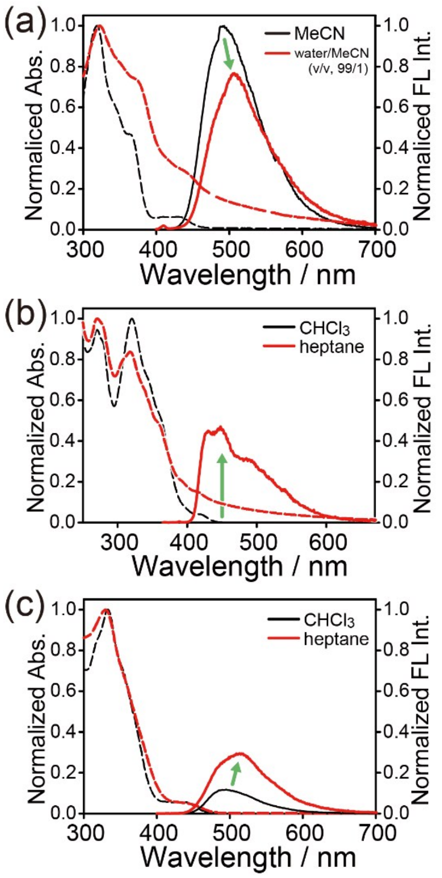

Fig. 5 Normalized fluorescence spectra of (a) compounds **2a** (black, in MeCN, λ_{max} = 493 nm; red, in water/MeCN = 99/1, λ_{max} = 507 nm; λ_{ex} = 360 nm), (b) **3a** (red, heptane, λ_{max} = 448 nm, λ_{ex} = 350 nm), and (c) **3b** (black, in $CHCl_3$, λ_{max} = 495 nm; red, in heptane, λ_{max} = 513 nm; λ_{ex} = 370 nm). The area of fluorescence spectrum was normalized based on fluorescence quantum yield of each compound. Green arrow denotes enhancement or suppression of fluorescence efficiency upon aggregation. Dashed lines denote corresponding normalized absorption spectra.

Fluorescence intensity of **3a** was significantly weak in the monomer state (no emission in $CHCl_3$ and Φ_f = 1%, $\lambda_{max,FL}$ = 454 nm in MCH) (Fig. 4b and 5b). In contrast to the monomer state, a prominent blue emission was clearly observed from the fibrous aggregates of **3a** formed in heptane (Φ_f = 8%, $\lambda_{max,FL}$ = 448 nm). It is noted that because of the weak fluorescent nature of the monomer state, a high-contrast fluorescence switching upon aggregation was achieved using compound **3a**.

By introducing additional two methoxy group at the 3- and 12-positions, monomer state becomes more emissive and a green fluorescence was observed from dilute solution of **3b** in $CHCl_3$ (Φ_f = 2%, $\lambda_{max,FL}$ = 495 nm) and MCH (Φ_f = 5%, $\lambda_{max,FL}$ = 480 nm) (Fig. 4c and 5c). Although the fluorescence quantum yield of the aggregates of **3b** in heptane (Φ_f = 5%) was comparable to that in MCH, a significant redshift in fluorescence maximum by 33 nm was observed upon aggregation of **3b** in heptane ($\lambda_{max,FL}$ = 513 nm) compared to that in MCH ($\lambda_{max,FL}$ = 480 nm).

Analysis based on kinetic constants

In order to gain insight into the origin of aggregation-induced enhancement or suppression of fluorescence property, two rate constants, i.e., fluorescence emission rate constant (k_f) and non-radiative decay rate constant (k_{nr}), were investigated.[42,43] Fluorescence quantum yield is the ratio of fluorescence emitting rate to the sum of the all decay rates as expressed by the following equation:

$$\Phi_f = \frac{k_f}{k_f + k_{nr}} = k_f \tau_f \qquad (1)$$

where the contribution of all non-radiative decay processes, including intersystem crossing, are involved in the k_{nr} value.[44] As is clear from equation (1), the Φ_f value becomes larger when the emission rate (k_f) gets larger or the non-radiative rate (k_{nr}) gets smaller. Therefore, the origin of fluorescence enhancement (suppression) can be categorized into two different types: (1) increase (decrease) of the k_f value and (2) decrease (increase) of the k_{nr} value.

The time-resolved fluorescence spectra of compounds **1a**, **2a**, **3a**, and **3b** in solution were monitored using a streak scope and the decay curve of fluorescence intensity was fitted by multi-exponential functions (See Fig. S11–S18 in the ESI† for details). The area weighted mean fluorescence lifetime ($<\tau_f>$) was then calculated from observed time constant and coefficient of each exponential component (Table S1 in the ESI†). Fluorescence quantum yield (Φ_f), area-weighted mean fluorescence lifetime

Table 1. Emission properties of compounds **1–3** in monomer and aggregated states.

compound	solvent	Φ_f	$<\tau_f>$ (ns)	k_f (ns^{-1})^a	k_{nr} (ns^{-1})^a
1a	CHCl$_3$	0.19	7.7	0.025	0.10
2a	MeCN	0.17	9.9	0.017	0.084
	water^b	0.13	12.0	0.011	0.073
3a	CHCl$_3$	n.d.^{c}	–^{c}	–^{c}	–^{c}
	MCH	0.01	1.7	0.006	0.59
	heptane	0.08	6.7	0.012	0.14
3b	CHCl$_3$	0.02	1.0	0.019	0.94
	MCH	0.05	2.6	0.019	0.37
	heptane	0.05	4.5	0.011	0.21

[a] Fluorescence emission rate constant (k_f) and non-radiative decay rate constant (k_{nr}) were calculated as follows: $k_f = \Phi_f/<\tau_f>$, $k_{nr} = (1 - \Phi_f)/<\tau_f>$. [b] In mixed solvent of water/MeCN (v/v, 99/1). [c] Emission was not detected.

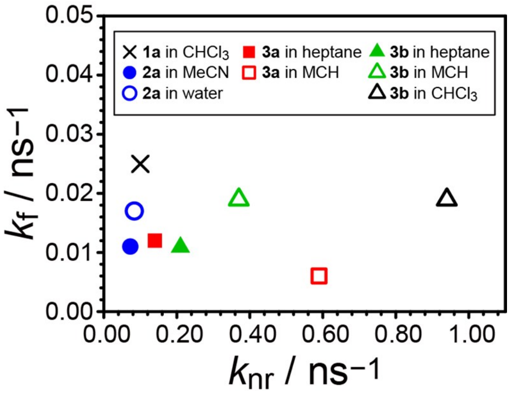

Fig. 6 Scatter plot of fluorescence emission rate constant (k_f) on the y axis and nonradiative decay rate constant (k_{nr}) on the x axis.

($<\tau_f>$), and the two rate constants (i.e., k_f and k_{nr}) determined from the Φ_f and $<\tau_f>$ values were summarized in Table 1.

Scatter plot of the k_f value on the y-axis and the k_{nr} value on the x-axis is shown in Fig. 6. By the scatter plot of the rate constants, the origin of fluorescence enhancement/suppression can be seen in a visually intuitive way: a highly emissive state appears on the upper-left part of this plot and a non-emissive state is on the lower-right part. Compound **2a** is plotted on the left part of the scatter plot (blue circle in Fig. 6), suggesting that the relatively high fluorescence quantum yield of **2a** (i.e., Φ_f = 0.17 in MeCN and 0.13 in the aqueous media) is associated with a small k_{nr} value compared to the other compounds. The aggregation-induced suppression of fluorescence for compound **2a**—that can be regarded as the downward shift of blue circle plot from the open to filled symbols in Fig. 6—is attributed to the decrease of k_f value upon forming the spherical aggregates in aqueous media. It is likely that the decrease of k_f originates from an intermolecular electronic interaction in the spherical aggregates, causing suppression of the emission process of **2a**.

In the case of compound **3b**, fluorescence quantum yield was significantly small in CHCl$_3$ (Φ_f = 0.02) where intermolecular interaction is absent and solvent effect is considered to be significant. The weak fluorescence of **3b** is attributed to large k_{nr} values (k_{nr} = 0.94 ns^{-1} in CHCl$_3$), which is clear from Fig. 6 that the black open triangle symbol is located at the right part on the scatter plot. In the monomer state in apolar solvent, fluorescence quantum yield of **3b** (Φ_f = 0.05 in MCH) was 2.5-times larger than that in CHCl$_3$, which is attributed to the decrease of k_{nr} value from 0.94 ns^{-1} in CHCl$_3$ to 0.37 ns^{-1} in MCH. The effect of aggregation of compound **3b** on its fluorescence property can be regarded as a shift to the lower left direction of the green triangle plot from the open to filled symbols in Fig. 6, which corresponds to the suppression of non-radiative decay process (i.e., decrease of k_{nr} value from 0.94 to 0.21 ns^{-1}) and the decrease of k_f value (from 0.019 to 0.011 ns^{-1}) upon forming fibrous aggregates of **3b** in heptane. Upon forming aggregates of compound **3b**, decreasing effect of k_f on Φ_f and increasing effect of k_{nr} cancel each other out, therefore, fluorescence quantum yield was comparable in MCH and heptane in the case of **3b**. It is noted that such decrease of k_f value upon aggregation was commonly observed for compounds **2a** and **3b**.

As described above, fluorescence quantum yield of compound **3a** in the monomer state is significantly small (no emission in CHCl$_3$ and Φ_f = 1% in MCH). By comparing the red open square plot (**3a** in MCH) to the green open triangle plot (**3b** in MCH) in Fig. 6, the weak fluorescence nature of **3a** can be attributed to both the small k_f and large k_{nr} values (k_f = 0.006 ns^{-1} and k_{nr} = 0.59 ns^{-1} in MCH). Upon aggregation of **3a** in heptane, both the two rate constants (i.e., k_f and k_{nr}) became comparable to those of compound **3b** as shown in the red and green filled symbols in Fig. 6. Thus, both the increase of k_f value and the decrease of k_{nr} cooperatively contributes the aggregation-induced enhancement of fluorescence in the case of **3a**.

Vibronic coupling density analysis

In order to clarify the reason why the monomer state of compound **3a** is significantly weak compared to **3b**, we calculated the ground and excited states of **3a** and **3b** at the B3LYP/6-31G(d) and TD-B3LYP/6-31G(d) levels of theory. All the octyl groups of compounds **3a** and **3b** were replaced by methyl group to simplify calculations.

Molecular orbital correlation diagram of compounds **3a** and **3b** is shown in Fig. 7. As shown in the diagram, HOMO and HOMO−1 of compounds **3a** and **3b** are localized in the (3,4,5-trialkoxyphenyl)carbamolyl moiety, while HOMO−2 and LUMO are localized in the [5]helicene core moiety. In the case

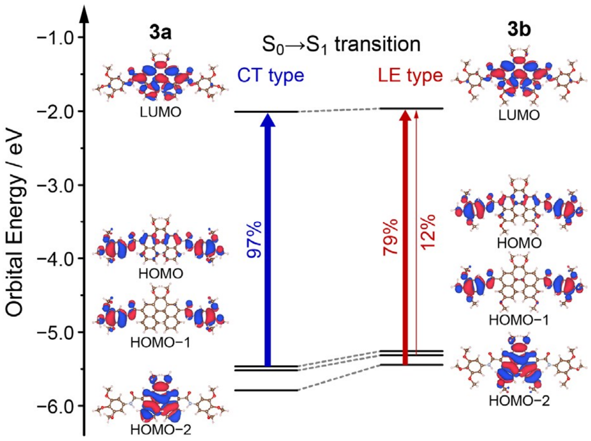

Fig. 7 Orbital correlation diagram of compounds **3a** and **3b** in the ground state (S$_0$) calculated at the TD-B3LYP/6-31g(d) level of theory. The blue and red arrows represent the lowest energy transition of **3a** (from HOMO to LUMO, charge-transfer (CT) type transition) and **3b** (mainly from HOMO−2 to LUMO, local-excitation (LE) type transition).

of compound **3a**, the lowest energy excitation is the transition from HOMO to LUMO (97%), suggesting that the lowest energy excited state (S_1) of **3a** has a charge transfer (CT) property. On the other hand, the methoxy substitution at the 3- and 12-positions of [5]helicene selectively raises the energy of HOMO−2, and HOMO−2 of compound **3b** locates close to HOMO and HOMO−1. Consequently, the lowest energy excitation of compound **3b** consists mainly of the transition from HOMO−2 to LUMO (79%), but not the HOMO-LUMO transition. Thus, the nature of S_1 state is significantly different between compounds **3a** and **3b**: the S_1 state of **3a** is of a CT type, while that of **3b** is of a local excitation (LE) type. Details of other electronic transitions of compounds **3a** and **3b** are summarized in Table S2 and S3 in the ESI†.

In order to gain further insight into the effect of methoxy substitution on the emission and non-radiative rate constants, vibronic coupling constants (VCC) and vibronic coupling density (VCD) analysis[45,46] of compounds **3a** and **3b** were carried out. The vibronic coupling calculations were performed by employing our in-house codes. The details of the method of calculations are described in elsewhere.[47,48] Diagonal and off-diagonal vibronic couplings are the driving force of a vibrational relaxation and a non-radiative transition, respectively.[47]

The diagonal VCCs for each normal mode of **3a** and **3b** are shown in Fig. 8a and 8b, respectively. We found that the number of large diagonal VCCs in **3a** is larger than that in **3b**. This is consistent with the large vibrational relaxation obtained from the excited-state optimisation of **3a** (Fig. S19–S23 in the ESI†). A large diagonal vibronic coupling gives rise to the reduction of the Franck-Condon factor to suppress the fluorescence.[47] Therefore, a small k_f value is expected for compound **3a** due to the large diagonal vibronic couplings.

VCD analysis provides a local picture of the interactions on the basis of the electronic and vibrational structures,[45] which enables us to assess the origin of VCCs.[48,49] The result of diagonal VCD analyses for **3a** and **3b** is shown in Fig. S24 and S25 in the ESI†, respectively. Since the electron density difference ($\Delta\rho$) of **3a** is strongly delocalized over the whole molecule, most vibrational modes in **3a** couple to the electronic state. On the other hand, the $\Delta\rho$ of **3b** is localized in the [5]helicene core moiety, suggesting that only the vibrational modes of the [5]helicene fragment can couple to the electronic state. Therefore, the number of the strong coupling modes is small in compound **3b**.

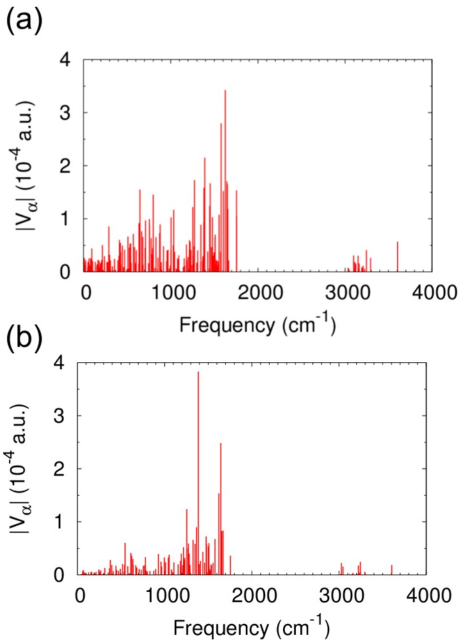

Fig. 8 Diagonal vibronic coupling constants for the normal modes of (a) **3a** and (b) **3b**.

This result indicates that [5]helicenes becomes non-fluorescent by introducing a donor substituent such as (3,4,5-trialkoxyphenyl)-carbamoyl group at the 5- and 10-positions, due to the CT-type transition in the lowest energy excited state. Compound **3a**—that shows only weak fluorescence in the monomer state—becomes moderately fluorescent upon aggregation, which may be due to suppression of the large vibrational relaxation at the S_1 state.

4 Conclusions

In this work, fluorescence properties of 5,10-disubstituted [5]helicene derivatives, which form aggregates in aqueous media or apolar solvent, were carefully investigated based on the radiative (k_f) and non-radiative (k_{nr}) rate constants for the decay of excited state. Upon forming aggregates, regardless of the type of self-assembly (i.e., spherical aggregates formed by hydrophobic interactions in aqueous media or fibrous aggregates formed by van der Waals interactions in apolar solvent), k_f slightly decreases due to intermolecular interaction inside aggregates. On the other hand, significant suppression of k_{nr} upon aggregation was observed only for the fibrous aggregates formed in apolar solvent, which is responsible for the aggregation-induced enhancement of fluorescence of compound **3a**. By introducing appropriate donor substituent to [5]helicene core (i.e., 3,4,5-trialkoxyphenylcarbamoyl group at the 5- and 10-positions), fluorescence quantum yield of [5]helicenes significantly decreased in the monomer state likely due to the CT-type property in the lowest energy excited state. The weakly fluorescent state can be altered to be more fluorescent (1) by introducing additional methoxy group at the 3- and 12-positions of [5]helicene or (2) by forming aggregates in solution phase. Dynamic helical inversion property of [5]helicenes by external stimuli, chiroptical properties enhanced by self-assembly, and design of a highly luminescent helicene derivative in aggregates are now under investigation in our group.

Acknowledgements

This research was supported by a Grant-in-Aid for Scientific Research on Innovative Areas "Photosynergetics" (No. 26107008), from the Ministry of Education, Culture, Sports, Science and Technology (MEXT), Japan. This work was also supported by a Grant-in-Aid for Young Scientists (B) (No. 25810048) and a Grant-in-Aid for Scientific Research (C) (No. 15K05607) from the Japan Society for the Promotion of Science (JSPS), Japan.

Notes and references

1 Y. Shen, C.-F. Chen., *Chem. Rev.*, 2012, **112**, 1463–1535.
2 M. Gingras, *Chem. Soc. Rev.*, 2013, **42**, 968–1006.
3 M. Gingras, G. Félix, R. Peresutti, *Chem. Soc. Rev.*, 2013, **42**, 1007–1050.
4 M. Gingras, *Chem. Soc. Rev.*, 2013, **42**, 1051–1095.
5 C. Schmuck, *Angew. Chem. Int. Ed.*, 2003, **42**, 2448–2452.
6 A. Urbano, *Angew. Chem. Int. Ed.*, 2003, **42**, 3986–3989.
7 K. Mori, T. Murase, M. Fujita, *Angew. Chem. Int. Ed.*, 2015, **54**, 6847–6851.
8 R. H. Martin, M. Baes, *Tetrahedron*, 1975, **31**, 2135–2137.
9 N. Ito, T. Hirose, K. Matsuda, *Org. Lett.*, 2014, **16**, 2502–2505.
10 S. Grimme, J. Harren, A. Sobanski, F. Vögtle, *Eur. J. Org. Chem.*, 1998, **1998**, 1491–1509.
11 E. M. Sánchez-Carnerero, A. R. Agarrabeitia, F. Moreno, B. L. Maroto, G. Muller, M. J. Ortiz, S. de la Moya, *Chem. Eur. J.*, 2015, **21**, 13488–13500.
12 Y. Nakai, T. Mori, Y. Inoue, *J. Phys. Chem. A*, 2012, **116**, 7372–7385.
13 F. Furche, R. Ahlrichs, C. Wachsmann, E. Weber, A. Sobanski, F. Vögtle, S. Grimme, *J. Am. Chem. Soc.*, 2000, **122**, 1717–1724.
14 J. B. Birks, D. J. S. Birch, E. Cordemans, E. Vander Donckt, *Chem. Phys. Lett.*, 1976, **43**, 33–36.
15 M. Sapir, E. Vander Donckt, *Chem. Phys. Lett.*, 1975, **36**, 108–110.
16 K. Schmidt, S. Brovelli, V. Coropceanu, D. Beljonne, J. Cornil, C. Bazzini, T. Caronna, R. Tubino, F. Meinardi, Z. Shuai, J.-L. Brédas, *J. Phys. Chem. A*, 2007, **111**, 10490–10499.
17 H. Sakai, S. Shinto, J. Kumar, Y. Araki, T. Sakanoue, T. Takenobu, T. Wada, T. Kawai, T. Hasobe, *J. Phys. Chem. C*, 2015, **119**, 13937–13947.
18 H. Oyama, K. Nakano, T. Harada, R. Kuroda, M. Naito, K. Nobusawa, K. Nozaki, *Org. Lett.*, 2013, **15**, 2104–2107.
19 K. Goto, R. Yamaguchi, S. Hiroto, H. Ueno, T. Kawai, H. Shinokubo, *Angew. Chem. Int. Ed.*, 2012, **51**, 10333–10336.
20 Y. Sawada, S. Furumi, A. Takai, M. Takeuchi, K. Noguchi, K. Tanaka, *J. Am. Chem. Soc.*, 2012, **134**, 4080–4083.
21 K. J. Dougherty, C. M. Kraml, N. Byrne, J. A. Porras, S. Bernhard, J. T. Mague, R. A. Pascal, Jr., *Tetrahedron*, 2015, **71**, 1694–1699.
22 S. Sahasithiwat, T. Mophuang, L. Menbangpung, S. Kamtonwong, T. Sooksimuang, *Synth. Met.*, 2010, **160**, 1148–1152.
23 J.-D. Chen, H.-Y. Lu, C.-F. Chen, *Chem. Eur. J.*, 2010, **16**, 11843–11846.
24 M. Li, Y. Niu, X. Zhu, Q. Peng, H.-Y. Lu, A. Xia, C.-F. Chen, *Chem. Commun.*, 2014, **50**, 2993–2995.
25 M. Li, W. Yao, J.-D. Chen, H.-Y. Lu, Y. Zhao, C.-F. Chen, *J. Mater. Chem. C*, 2014, **2**, 8373–8380.
26 Y. Dai, T. J. Katz, D. A. Nichols, *Angew. Chem. Int. Ed. Engl.*, 1996, **35**, 2109–2111.
27 T. Verbiest, S. Van Elshocht, M. Kauranen, L. Hellemans, J. Snauwaert, C. Nuckolls, T. J. Katz, André Persoons, *Science*, 1998, **282**, 913–915.
28 K. E. S. Phillips, T. J. Katz, S. Jockusch, A. J. Lovinger, N. J. Turro, *J. Am. Chem. Soc.*, 2001, **123**, 11899–11907.
29 M. T. Stone, J. M. Fox, J. S. Moore, *Org. Lett.*, 2004, **6**, 3317–3320.
30 T. Kaseyama, S. Furumi, X. Zhang, K. Tanaka, M. Takeuchi, *Angew. Chem. Int. Ed.*, 2011, **50**, 3684–3687.
31 N. Saleh, C. Shen, J. Crassous, *Chem. Sci.*, 2014, **5**, 3680–3694.
32 J. Kumar, T. Nakashima, T. Kawai, *J. Phys. Chem. Lett.*, 2015, **6**, 3445–3452.
33 D. C. Harrowven, I. L. Guy, L. Nanson, *Angew. Chem. Int. Ed.*, 2006, **45**, 2242–2245.
34 C. V. Yelamaggad, A. S. Achalkumar, D. S. Shankar Rao, S. K. Prasad, *J. Org. Chem.*, 2007, **72**, 8308–8318.
35 F. J. M. Hoeben, P. Jonkheijm, E. W. Meijer, A. P. H. J. Schenning, *Chem. Rev.*, 2005, **105**, 1491–1546.
36 F. Würthner, *Chem. Commun.*, 2004, 1564–1579.
37 Y. Kim, W. Li, S. Shin, M. Lee, *Acc. Chem. Res.*, 2013, **46**, 2888–2897.
38 T. Hirose, F. Helmich, E. W. Meijer, *Angew. Chem. Int. Ed.*, 2013, **52**, 304–309.
39 T. Hirose, K. Matsuda, *Org. Biomol. Chem.*, 2013, **11**, 873–880.
40 Y. Nagata, T. Nishikawa, M. Suginome, *J. Am. Chem. Soc.*, 2014, **136**, 15901–15904.
41 Y. Nakano, T. Hirose, P. J. M. Stals, E. W. Meijer, A. R. A. Palmans, *Chem. Sci.*, 2012, **3**, 148–155.
42 T. Hirose, Y. Tsunoi, Y. Fujimori, K. Matsuda, *Chem. Eur. J.*, 2015, **21**, 1637–1644.
43 T. Hirose, K. Higashiguchi, K. Matsuda, *Chem. Asian J.*, 2011, **6**, 1057–1063.
44 N. J. Turro, V. Ramamurthy, J. C. Scaiano, *Principles of Molecular Photochemistry: An Introduction*, University Science Books, Sausalito, CA, 2009.
45 T. Sato, K. Tokunaga, K. Tanaka, *J. Phys. Chem. A*, 2008, **112**, 758–767.
46 T. Sato, N. Iwahara, K. Tanaka, *J. Phys. Conf. Ser.*, 2013, **428**, 012003 1–7.
47 M. Uejima, T. Sato, D. Yokoyama, K. Tanaka, J.-W. Park, *Phys. Chem. Chem. Phys.* 2014, **16**, 14244–14256.
48 M. Uejima, T. Sato, K. Tanaka, H. Kaji, *Chem. Phys.* 2014, **430**, 47–55.
49 M. Uejima, T. Sato, M. Detani, A. Wakamiya, F. Suzuki, H. Suzuki, T. Fukushima, K. Tanaka, Y. Murata, C. Adachi, H. Kaji, *Chem. Phys. Lett.*, 2014, **602**, 80–83.

Graphical Abstract

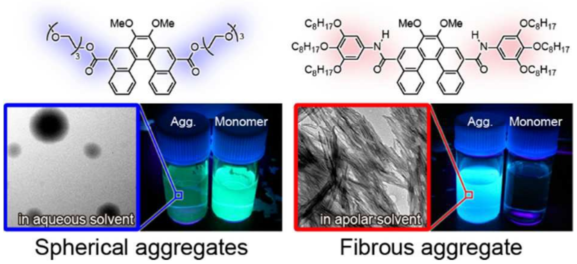

Fluorescence behavior of 5,10-disubstituted [5]helicene derivatives is sensitive to the type of substituents and the motif of self-assembly in solution phase.